Contrib Mineral Petrol (1994) 115:384–401

Contributions to Mineralogy and Petrology

Mineralogical and geochemical study of granular xenoliths from the Alban Hills volcano, Central Italy: bearing on evolutionary processes in potassic magma chambers

M. Federico[1], A. Peccerillo[2], M. Barbieri[1], and T.W. Wu[3]

[1] Dipartimento di Scienze della Terra, University "La Sapienza", Roma, Italy
[2] Istituto di Scienze della Terra, University of Messina, C.P. 54, 98166 Messina-S. Agata, Italy
[3] Department of Geology, University of Western Ontario, London, Ontario, Canada

Received January 4, 1993 / Accepted September 13, 1993

Abstract. Granular xenoliths (ejecta) from pyroclastic deposits emplaced during the latest stages of activity of the Alban Hills volcano range from ultramafic to salic. Ultramafic types consist of various proportions of olivine, spinel, clinopyroxene and phlogopite. They show low SiO_2, alkalies and incompatible element abundances and very high MgO. However, Cr, Co and Sc are anomalously low, at a few ppm level. Olivine is highly magnesian (up to Fo% = 96) and has rather high CaO (1% Ca) and very low Ni (around a few tens ppm) contents. These characteristics indicate a genesis of ultramafic ejecta by thermal metamorphism of a siliceous dolomitic limestone, probably with input of chemical components from potassic magma. The other xenoliths have textures and compositional characteristics which indicate that they represent either intrusive equivalents of lavas or cumulates crystallized from variably evolved ultrapotassic magmas. One sample of the former group has major element composition resembling ultrapotassic rocks with kamafugitic affinity. Some cumulitic rocks have exceedingly high abundances of Th (81–84 ppm) and light rare-earth elements (LREE) (La + Ce = 421–498 ppm) and extreme REE fractionation (La/Yb = 288–1393), not justified by their modal mineralogy which is dominated by sanidine, leucite and nepheline. Fine-grained phases are dispersed through the fractures and within the interstices of the main minerals. Semiquantitative EDS analyses show that Th and LREE occur at concentration levels of several tens of percent in these phases, indicating that their presence is responsible for the high concentration of incompatible trace elements in the whole rocks. The interstitial position of these phases and their association with fluorite support a secondary origin by deposition from fluorine-rich fluids separated from a highly evolved potassic liquid. The Nd isotopic ratios of the ejecta range from 0.51182 to 0.51217. $^{87}Sr/^{86}Sr$ ratios range from 0.70900 to 0.71036. With the exception of one sample, these values are lower than those of the outcropping lavas, which cluster around 0.7105 ± 3. This indicates either the occurrence of several isotopically distinct potassic magmas or a variable interaction between magmas and wall rocks. However, this latter hypothesis requires selective assimilation of host rocks in order to explain isotopic and geochemical characteristics of lavas and xenoliths. The new data indicate that the evolutionary processes in the potassic magmas of the Alban Hills were much more complex than envisaged by previous studies. Interaction of magmas with wall rocks may be an important process during magmatic evolution. Element migration by gaseous transfer, often invoked but rarely constrained by sound data, is shown to have occurred during the latest stages of magmatic evolution. Such a process was able to produce selective enrichment of Th, U, LREE and, to a minor degree, Ta and Hf in the wall rocks of potassic magma chamber. Finally, the occurrence of xenoliths with kamafugitic composition points to the existence of this type of ultrapotassic magma at the Alban Hills.

Correspondence to: A. Peccerillo

Introduction

Recent studies on potassic and ultrapotassic rocks have shown that their compositional characteristics can furnish information on a number of geological processes, such as element migration through upper mantle (mantle metasomatism), recycling of upper crustal material along subduction zones, intra-mantle contamination of basaltic magmas and the intimate nature of the mechanisms of mantle melting during the generation of various basaltic magmas (e.g., Ellam and Cox 1991; Foley 1992; Nelson 1992).

However, a crucial point in the use of potassic magmas as indicators of mantle processes is first to understand the extent to which primary compositions have been modified during rise to the surface. The Roman Comagmatic Province of Central Italy is a key region wherein to investigate this topic. This area has been the site of extensive, recent to active, potassic magmatism,

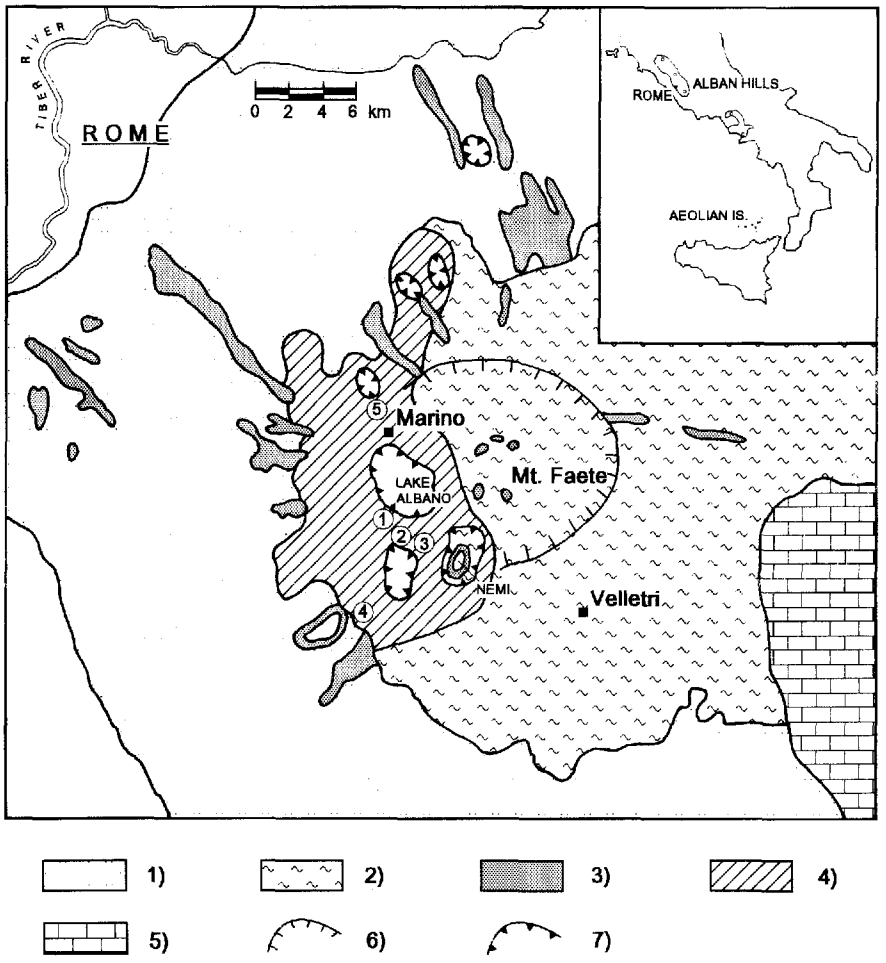

Fig. 1. Sketch map of the Alban Hills. *1*, Pre- and syn-caldera pyroclastics; *2*, post-caldera pyroclastics; *3*, main lava flows; *4*, late hydrovolcanic deposits; *5*, sedimentary rocks of the basement; *6*, caldera rim; *7*, explosion crater rim. *Numbers* on the map indicate sampling points: *1*, Cappuccini (P23); *2*, Ponte Albano, Ariccia (P30); *3*, Parco Chigi, Ariccia (P25, P10, P6); *4*, Villafranca (P14, P34); *5*, Colle Cimino (BD, KLT)

which built up both monogenic and large composite volcanoes. All the Roman rocks, including the most mafic ones, display striking crustal-like geochemical and isotopic signatures, whose origin has been the subject of debate. Early hypotheses suggested that interaction between "normal" magmas and carbonate wall rocks was responsible for the most outstanding petrological characteristics of Roman rocks (Rittman 1933). The role of continental crust has been emphasized by several other studies (e.g., Turi and Taylor 1976); a crustal origin for the largely predominant phonolitic rocks has been suggested by Vollmer (1989). Other processes such as gaseous transfer also have been invoked to explain the extreme enrichments in some incompatible elements in potassic rocks (e.g., Villemant 1988).

On the other hand, several recent studies have argued that the most prominent compositional characteristics of potassic magmas have to be related to a genesis in an anomalous source which has suffered metasomatic modifications by the addition of subduction-related upper crustal material (see Peccerillo 1990, for a review). Yet, there is still uncertainty on the extent to which low-pressure processes may have modified the compositional characteristics of potassic magmas.

The present paper aims to investigate the nature and geochemical effects of evolutionary processes in potassic magma chambers by an integrated mineralogical, petrological, trace element and isotopic (Sr, Nd) study of a suite of granular ejecta collected from some of the youngest pyroclastic formations at the Alban Hills (Central Italy) (Fornaseri 1951; Federico 1976). The rationale behind this investigation is that studies on ejecta are able to furnish information on magmatic processes that is less easily achieved from studies of lavas and the juvenile component of pyroclastic rocks (e.g., Barbieri et al. 1975; Hermes and Cornell 1981, 1983; Varekamp 1983; Turbeville 1992).

The rocks studied include a number of lithologies which point to variable origins within the volcanic system. The processes responsible for xenolith generation and the effects of these processes on compositional variations in ultrapotassic liquids are discussed.

Volcanological outlines and previous studies

The Alban Hills are a huge composite volcano with a central caldera, situated south-east of Rome. The volcano consists entirely of ultrapotassic pyroclastics and minor lavas belonging to the so-called High-K Series (HKS) of the Roman Province. The age of the deposits ranges between at least 530 ka and 30 ka (Bernardi et al. 1982). Previous investigations recognized two main stages of activity, separated by a huge ignimbrite eruption responsible for the formation of the summit caldera (Fornaseri et al. 1963; De Rita et al. 1988) (Fig. 1). Rock compositions range from leucite tephrite to leucite phonolite, all with high to extreme enrichments

in K and incompatible trace elements (Fornaseri et al. 1963; Peccerillo et al. 1984). The Sr isotopic ratios of lavas have been found to cluster around 0.7105 ± 3, whereas $\delta^{18}O$ ‰ values range from $+5.9$ to $+7.8$ (Ferrara et al. 1985).

The Alban Hills rest on a thick pile (about 2500 m) of sedimentary rocks that include Mesozoic and Cenozoic marls, limestones and dolomites, Cenozoic and Quaternary clays, marls and sandstones (Funiciello and Parotto 1978).

The Alban Hills ejecta

The occurrence of ejecta in the pyroclastic formations from the Alban Hills has been well known for a long time (Lacroix 1917; Washington 1927). The xenoliths include sedimentary, mostly carbonatic, metamorphic and igneous types. Granular xenoliths with igneous-like textures include a large variety of lithologies which range from ultramafic to salic.

The samples studied in this paper consist of nine xenoliths, which have been selected from a more abundant population collected and studied by Fornaseri (1951), Fornaseri et al. (1963) and Federico (1976). The samples range from ultramafic to salic and span the whole compositional range of the granular ejecta studied by previous investigations. Most of the samples come from the wet pyroclastic flows (lahars) cropping out around the explosion craters of Lago Albano and Valle Ariccia; BD and KLT ejecta were collected from the Monte Cimino scoria cone. Both these pyroclastic formations belong to the latest phases of the Alban Hills activity. Sample localities are shown in Fig. 1.

Petrography

All the samples under study have a granular texture, a rounded to irregular shape and a size ranging from a few cm to more than 0.5 m. Some of them show an uneven distribution of the main phases. Modes are reported in Table 1.

Sample BD consists of olivine and spinel. Olivine is present as undeformed, coarse- to medium-grained, anhedral to subhedral crystals, poikilitically enclosing several euhedral crystals of light brown spinel. Spinel also occurs as aggregates of subhedral to euhedral, fine- to medium-grained crystals. Some fluid inclusions are observed in olivine.

Samples P34 and P14 have an autoallotriomorphic granular texture, with some triple points. Olivine occurs both as large anhedral crystals with numerous mineral and fluid inclusions, and as small euhedral to slightly rounded grains often included in brown mica. Clinopyroxene is subhedral and colourless and often contains spinel, olivine and brown mica. Mica consists of large crystals poikilitically containing olivine and spinel. Spinels are euhedral, deep green, and occur both as inclusions of single crystals in olivine and as aggregates.

No glass inclusions have been observed in BD, P34 and P14.

Sample P6 has a subidiomorphic granular texture and consists of dominant clinopyroxene and leucite with minor hauyne-nosean. Dark mica, apatite, amphibole, feldspar and opaque minerals (magnetite and pyrrhotite) are present in minor or accessory amounts. Clinopyroxenes occur as idiomorphic, slightly elongated pale green crystals, with deep green, strongly pleochroic rims. Trains of fluid and glassy inclusions, apatite, and dark mica are enclosed in pyroxenes. Leucite and hauyne-nosean are subhedral to anhedral and contain inclusions of opaque minerals, apatite, needle-like and granular pyroxene crystals. Elongated feldspars are interstitial. A partially transformed, fine-grained aggregate of minerals, in which ghosts of feldspars are still recognizable, occupies the interstices.

Sample KLT (kalsilitolite) has clinopyroxene phenocrysts and megacrysts in a medium-grained matrix of clinopyroxene, garnet, brown mica, with large amounts of interstitial kalsilite. The largest clinopyroxene crystals are optically homogeneous and have strongly resorbed rims which contain several garnet and mica inclusions. The smaller phenocrysts are euhedral to subhedral, with patchy extinction and numerous dark mica and garnet inclusions. Clinopyroxene crystals free from inclusions are also observed and, in some cases, small crystals are included within the garnet. Kalsilite is invariably perthitic with exsolved nepheline (Aurisicchio and Federico 1985). Garnet occurs as isolated crystals, as aggregates and as small grains included in clinopyroxene. Some garnet crystals are partially or completely transformed to a fine-grained aggregate of magnetite, dark mica and clinopyroxene. Dark mica is mostly found both as large anhedral crystals and as thin lamellae included in the clinopyroxene. Apatite and opaque minerals occur as accessories. Some fluorite has been observed.

Sample P10 consists of dominant sanidine, nepheline, leucite and amphibole, with minor clinopyroxene, garnet, dark mica and accessory hauyne-nosean, magnetite and pyrrhotite. Sanidine is present as elongated crystals often including clinopyroxene, garnet, hauyne-nosean and mica. Clinopyroxene is colorless to green and is sometimes transformed to amphibole and mica at the rim. Dark mica occurs as deep green, strongly pleochroic, large crystals. Garnet is yellowish, sometimes with color zoning and occurs both in aggregates and as isolated crystals, sometimes enclosed in other minerals such as leucite. Deep green amphibole occurs as single crystals and as a reaction product of clinopyroxene. Leucite forms large crystals often containing inclusions of mica, garnet, apatite and amphibole. Hauyne-nosean is found as small euhedral crystals.

Sample P30 has a granular texture and is composed of clinopyroxene and foids with accessory apatite, magnetite and brown mica. Clinopyroxene is euhedral to subhedral and displays color zoning from light green or colorless cores to deep green rims. They contain numerous fluid and mineral inclusions. The latter mostly consist of apatite and mica. Foids are interstitial and comprise subidiomorphic and idiomorphic crystals of leucite and minerals of sodalite group (hauyne-nosean) crowded with small dark inclusions.

Sample P25 consists of large leucite crystals associated with sanidine and nepheline, amphibole, garnet, brown mica, hauyne-nosean and fluorite. Leucite crystals are subidiomorphic and contain numerous fluid, glassy and mineral (cpx, apatite, opaque mineral) inclusions. Sanidine consists of euhedral, elongated crystals sometimes perthitic and enclosing leucite. Garnet is brown-yellowish in color, euhedral to anhedral. Brown mica is found as strongly pleochroic lamellae, sometimes enclosed in sanidine and leucite. Amphibole is deep green and pleochroic. It is often associated with mica or enclosed within leucite and garnet. Hauyne-nosean consists of small euhedral interstitial crystals and as inclusions in garnet and feldspar.

Sample P23 is made up of sanidine and nepheline with accessory amounts of amphibole and secondary fluorite. Sanidine occurs as large subhedral or euhedral tabular crystals. Nepheline is anhedral and contains numerous dusty inclusions along fractures. Amphi-

Table 1. Point counted modes for the studied xenoliths

	Ks	Sa	Ne	Lc	Sgm	Cpx	Amp	Ol	Mi	Gr	Sp	Fl	Acc
BD								62			38		
P34						1		25	58		15		<1
P14						22		35	26		16		<1
P6		<1		42	4	43	2		2				6
KLT	36					51			3	7	<1		2
P10		20	21	16	<1	7	20		6	7			2
P30				20	1	78			<1				<1
P25		14	18	57	1	<1	2			5	2		
P23		76	21	<1			<1				2		<1

Ks, kalsilite; Sa, sanidine; Ne, nepheline; Lc, leucite; Sgm, sodalite group minerals (nosean-hauyne); Cpx, clinopyroxene; Amp, amphibole; Ol, olivine; Mi, brown mica; Gr, garnet; Sp, spinel; Fl, fluorite; Acc, accessories (apatite, opaques)

bole is present only as thin elongated crystals included within sanidine and nepheline. A few grains of opaque minerals are also observed.

Mineral chemistry

Mineral compositions were determined at the Department of Earth Sciences, University of Rome on a Jeol JXA-50 electron microprobe fitted with an energy-dispersive system (EDS; Link System Ltd., type 860) and ZAF-4/FLS quantitative software. Operating conditions were: 15 kV accelerating voltage, 2 nA sample current and 100 seconds counting time. Fluorine-bearing phases were analyzed on a Cameca SX50 machine (15 kV, 15 nA and 100 s counting time) equipped with five wave-length dispersive (WDS) spectrometers and a Link eXL energy-dispersive system controlled by Specta software. Compositions of the most important mineral phases are reported in Table 2. A complete set of mineral analyses can be obtained from the senior author on request.

Mafic minerals include olivine, spinel, clinopyroxene, brown mica, garnet and amphibole.

Olivine (Table 2a) is unzoned and strongly magnesian (Fo% = 96–90). The CaO content is very high in BD olivine and decreases in P34 and P14, showing an anticorrelation with MnO and FeO. The NiO is low: Proton Induced X-ray Emission (PIXE) analyses (Santo et al. 1992) of olivine crystals indicated Ni contents invariably below the detection limit of a few tens ppm. All the olivines have CaO/MgO values which do not fit any of the trends reported by Ferguson (1978) for olivines of potassic igneous suites. Furthermore, our olivines are much more magnesian than olivines from Italian potassic lavas, with the only possible exception of Torre Alfina lamproites in which Fo% up to 93 has been found (Conticelli and Peccerillo 1990). Values of Fo_{92} have been found by Cundari (1982) in olivines from pyroxenite nodules at Vesuvius. Olivines from P34 and P14 contain high Zn concentrations.

Clinopyroxene (Table 2b) occurs in all the analyzed ejecta, except BD and P23, spanning a very large compositional range. Most define a continuous compositional trend (Fig. 2), similar to that for clinopyroxenes from Roman HKS volcanics (e.g., Scott Baldridge et al. 1981; Holm 1982; Aurisicchio et al. 1988). Clinopyroxenes from the ultramafic nodules P34 and P14 have high CaO/(MgO + FeO) values and define a separate group in the diagram of Fig. 2. Notably, these minerals do not show the compositional and color zoning, typical of clinopyroxenes from potassic lavas; Mg/(Mg + Fe) ratios are high, reflecting those in the coexisting olivines, whereas Fe^{2+}/Fe^{3+} (0.02–0.3) show the lowest values found in the analyzed clinopyroxenes; the M2 site is almost completely occupied by Ca, whereas the highest contribution of Al^{VI} to M1 site occupancy is observed. Clinopyroxenes from the other inclusions are zoned and tend to become increasingly Fe-rich in the sequence P30 to P10, KLT, P6, and P25, in which Fe-salite compositions are attained.

Mica (Table 2c) is found in almost all the analyzed ejecta. Micas from P34, P14, KLT and P30 can be classified as phlogopites, whereas those from the other samples are biotites (Bailey 1984). All have $Al^{IV}/Si > 0.33$, $Al^{VI} \leq 0.52$ and $Al^{IV} = 2.39$–2.65 atoms per formula unit.

Table 2a. Representative electron microprobe analyses and structural formulae of olivines in the Alban Hills ejecta

	BD		P34		P14	
SiO_2	41.37		41.42		40.88	
Al_2O_3	0.29		–		–	
FeO[a]	3.67		6.35		9.13	
MnO	0.24		0.47		0.46	
MgO	52.79		50.54		48.53	
CaO	1.06		0.74		0.58	
NiO	–		–		–	
ZnO	–		0.34		–	
Na_2O	0.25		0.32		0.14	
K_2O	–		0.05		–	
Total	99.67		100.23		99.72	
Numbers of ions on the basis of 4 oxygens						
Si	0.993		1.002		1.004	
Al	0.008		–		–	
Fe^{2+}	0.074		0.129		0.187	
Mn	0.005		0.010		0.010	
Mg	1.890	2.016	1.823	2.004	1.777	1.996
Ca	0.027		0.019		0.015	
Ni	–		–		–	
Zn	–		0.006		–	
Na	0.012		0.015		0.007	
K	–		0.002		–	
Fo	96.2		93.4		90.5	
Fa	3.8		6.6		9.5	

–, Below detection limit
[a] Total Fe as FeO

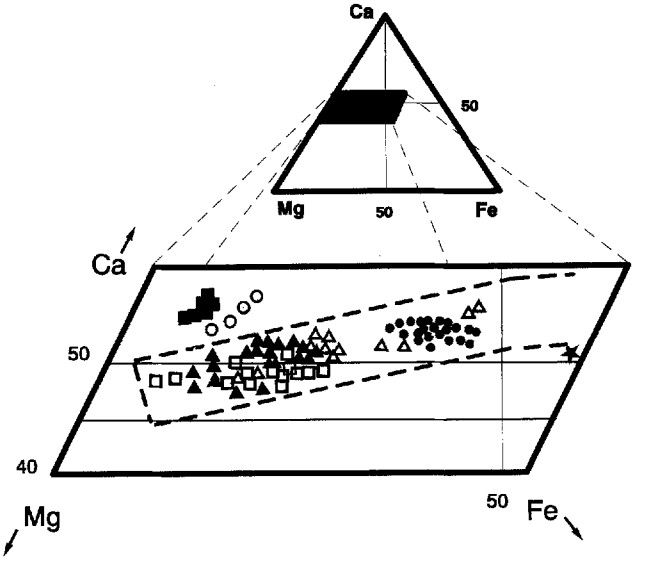

Fig. 2. Ca – Fe – Mg diagram for pyroxenes from the Alban Hills ejecta. Symbols: *star*, P25; *dots*, P6; *open triangles*, P10; *full triangles*, P30; *open squares*, KLT; *open circles*, P14; *full squares*, P34. *Heavy dashed lines* enclose the field of clinopyroxenes from the Alban Hills lavas (from Aurisicchio et al. 1988)

The highest Al^{VI} values are shown by micas of samples P34 and P14, reflecting the high Al^{VI} of the coexisting clinopyroxenes. Phlogopites associated with olivine have the highest Mg/Fe ratios. Their Ti contents are generally

Table 2b. Representative electron microprobe analyses and structural formulae of pyroxenes in the Alban Hills ejecta

	P34 Core	P34 Rim	P14 Core	P14 Rim	P30 Core	P30 Rim	P6 Core	P6 Rim	P10 Core	P10 Rim	KLT Core	KLT Rim	P25
SiO_2	47.40	47.20	48.12	47.08	49.36	47.34	43.57	40.67	48.94	45.31	52.68	51.32	42.60
TiO_2	0.82	1.00	0.72	0.52	0.69	1.56	1.45	2.08	0.79	1.31	0.19	0.37	1.42
Al_2O_3	9.08	9.08	8.20	8.90	4.32	5.04	8.50	10.55	3.97	7.82	1.39	2.50	8.91
Cr_2O_3	–	–	0.10	–	0.13	0.22	–	0.14	0.30	–	0.07	–	–
FeO[a]	3.49	3.71	3.48	4.31	5.98	8.21	11.07	12.01	6.85	8.76	7.01	8.17	15.83
MnO	–	–	–	0.06	0.11	0.20	0.26	0.26	–	–	0.25	0.15	0.60
MgO	13.81	13.76	13.44	13.24	13.70	11.98	9.71	8.86	13.44	11.84	13.80	12.99	6.70
CaO	25.54	25.31	25.15	25.08	24.15	24.23	24.16	23.48	24.29	24.21	23.81	23.64	22.52
Na_2O	–	–	0.25	0.16	0.72	0.52	0.50	0.46	0.40	0.21	0.45	0.61	0.43
Total	100.14	100.06	99.46	99.35	99.16	99.30	99.22	98.51	98.98*	99.46	100.21*	110.19*	99.01
Fe_2O_3[b]	3.80	3.70	2.93	4.54	5.73	5.80	9.47	10.89	5.07	7.23	1.44	3.22	7.80
FeO[b]	0.08	0.38	0.85	0.23	0.83	3.00	2.56	2.23	2.30	2.26	5.72	5.28	8.82
Numbers of ions on the basis of 6 oxygens													
Si	1.730	1.726	1.769	1.735	1.830	1.778	1.652	1.560	1.829	1.696	1.959	1.912	1.657
Al^{IV}	0.270	0.274	0.231	0.265	0.170	0.222	0.348	0.440	0.171	0.304	0.041	0.088	0.343
Al^{VI}	0.121	0.117	0.124	0.122	0.019	0.001	0.032	0.037	0.004	0.041	0.020	0.021	0.065
Ti	0.023	0.027	0.020	0.014	0.019	0.044	0.041	0.060	0.022	0.037	0.005	0.010	0.042
Cr	–	–	0.003	–	0.004	0.007	–	0.004	0.002	–	0.002	–	–
Fe^{3+}	0.104	0.102	0.081	0.126	0.160	0.164	0.270	0.314	0.142	0.203	0.040	0.090	0.228
Fe^{2+}	0.002	0.012	0.026	0.007	0.026	0.094	0.081	0.072	0.072	0.071	0.178	0.164	0.287
Mn	–	–	–	0.002	0.003	0.006	0.008	0.008	–	–	0.008	0.005	0.020
Mg	0.751	0.750	0.737	0.727	0.757	0.671	0.549	0.507	0.749	0.661	0.765	0.721	0.388
Ca	0.999	0.992	0.991	0.990	0.960	0.975	0.982	0.965	0.973	0.971	0.949	0.944	0.938
Na	–	–	0.018	0.011	0.052	0.038	0.037	0.034	0.029	0.015	0.032	0.044	0.032
mg[c]	0.997	0.985	0.966	0.990	0.967	0.877	0.871	0.876	0.912	0.903	0.811	0.814	0.575
Mg	40.5	40.4	40.2	39.3	39.7	35.1	29.0	27.2	38.7	34.7	39.4	37.5	20.9
ΣFe[d]	5.7	6.1	5.8	7.3	9.9	13.8	19.0	21.1	11.1	14.4	11.7	13.5	28.7
Ca	53.8	53.5	54.0	53.5	50.4	51.1	52.0	51.7	50.3	50.9	48.9	49.0	50.4
Na	0.0	0.0	6.6	3.9	21.5	12.5	8.6	6.4	13.1	4.3	41.4	30.9	7.8
Al^{IV}	92.3	90.9	85.9	91.1	70.5	73.0	81.7	82.4	76.9	85.3	51.8	61.9	82.3
Ti	7.7	9.1	7.4	5.0	8.0	14.5	9.7	11.2	10.0	10.4	6.8	7.3	9.9
									* Contains $ZrO_2 = 0.19$		* Contains ZnO = 0.19 SrO = 0.29 NiO = 0.08	* Contains NiO = 0.24 SrO = 0.20	

–, Below detection limit
[a] Total Fe as FeO
[b] Calculated according to Papike et al. 1974
[c] $mg = Mg/(Mg + Fe^{2+})$
[d] $\Sigma Fe = Fe^{2+} + Fe^{3+} + Mn$.

Table 2c. Representative electron microprobe analyses and structural formulae of micas in the Alban Hills ejecta

	P34	P14	P30	P6	P10	KLT	P25
SiO_2	38.93	38.38	38.13	35.33	36.89	35.06	35.47
TiO_2	0.94	0.95	1.69	1.32	1.61	3.68	1.26
Al_2O_3	17.97	18.67	15.45	19.17	15.35	14.90	14.13
Cr_2O_3	–	0.02	0.09	0.12	–	–	–
FeO[a]	3.58	5.26	8.35	20.84	17.81	12.07	23.49
MnO	–	0.02	–	0.29	0.30	0.22	1.56
MgO	23.00	22.56	20.59	11.48	13.58	17.26	9.23
CaO	–	0.01	0.03	0.17	0.03	–	0.08
BaO	0.30	0.07	1.15	1.59	–	4.36	–
ZnO	–	0.03	–	–	0.08	–	–
Na_2O	0.25	0.19	0.26	0.36	0.15	0.24	0.46
K_2O	10.14	10.39	9.58	9.01	9.61	9.00	9.50
Totals	95.41	96.55	95.32	96.00	95.41	96.79	95.18
Numbers of ions on the basis of 22 oxygens							
Si	5.520	5.408	5.565	5.476	5.593	5.294	5.609
Ti	0.100	0.101	0.185	0.154	0.184	0.418	0.150
Al^{IV}	2.480	2.592	2.435	2.524	2.407	2.652	2.391
Al^{VI}	0.523	0.508	0.222	0.328	0.336	–	0.242
Cr	–	0.002	0.010	–	–	–	0.014
Fe	0.425	0.620	1.019	2.702	2.258	1.524	3.106
Mn	–	0.002	–	0.038	0.039	0.028	0.209
Mg	4.862	4.739	4.480	2.653	3.070	3.886	2.176
Ca	–	0.002	0.005	0.028	0.005	–	0.014
Ba	0.017	0.004	–	0.097	–	0.258	–
Zn	–	0.003	0.044	–	0.009	–	–
Na	0.069	0.052	0.074	0.108	0.044	0.070	0.141
K	1.834	1.867	1.784	1.782	1.859	1.734	1.916
mg	0.920	0.884	0.815	0.495	0.576	0.718	0.410
F	0.89	0.31	1.64	1.09	1.41	1.34	2.05

–, Below detection
[a] Total Fe as FeO

low. Fluorine is rather low in phlogopites from P14 and P34 and increases in abundance in P30 phlogopite and in the biotites where values around 2% are found. The KLT micas show high TiO_2 (around 3.7%) and BaO (around 4.3%) abundances. It is noteworthy that amphiboles and apatites associated with biotites also have high F contents. The phlogopites compositionally resemble those in xenoliths from Vesuvius (Cundari 1982) and the Eifel (Lloyd and Bailey 1975).

Spinels from P34 and P14 have higher FeO_{total} and lower MgO than those in BD. Their Fe^{2+}/Fe^{3+} ratios are around 1.2–1.3 in the cores of spinels from P14 and P34, in contrast to the very low values found in the cores of the associated clinopyroxenes (0.321–0.019). This may record changes in the oxygen fugacity during crystallization. The Mg/Fe ratios are very high in BD, but become lower in the other samples which display values typical of spinels from Somma Vesuvius pyroxenitic inclusions (Cundari 1982). A high Zn content is observed in P14 spinel, reflecting the same characteristic in the associated olivine.

Garnet is melanitic in composition. Crystals from P25 and P10 are weakly zoned, with a small but consistent rimward increase in Si and Fe and decrease in Ti and Al. Garnets from KLT show a rimward increase in Si and Al and decrease in Ti and Fe. High Zr concentrations have been found in some crystals, in keeping with the occurrence of Zr-rich clinopyroxenes (Federico et al. 1988) and of baddeleyite (Gianfagna 1985) in some ejecta from the Alban Hills.

Amphibole (Table 2d) occurs both as primary single crystals and as reaction products of clinopyroxene. Compositions are hastingsite (P23) and magnesian hastingsite (P25, P10, P6), according to the classification of Leake (1978), with rather high K_2O and F contents. The latter reaches its maximum abundance in P25 (F = 1.11%), in which F-rich biotites and apatites have been found.

Salic minerals include K-feldspar, leucite, kalsilite, members of the sodalite group and nepheline.

K-feldspars (Table 2e) have Na_2O abundances ranging between <1% and 2.3%. Strontium abundances are high.

Leucites and nephelines are very similar in composition to those from lavas. The K/Na ratios of nephelines range from 0.227 to 0.294.

Kalsilite microperthites have a bulk composition of $Ks_{86.5}-Ne_{12.4}-Qz_{1.1}$, whereas the composition of the single exsolved phases range from $Ne_{4.98}-Ks_{95.02}$ to $Ne_{72.48}-Ks_{24.37}-Qz_{3.15}$ (Aurisicchio and Federico 1985).

Members of the *sodalite group (hauyne-nosean)* (Table 2f) have variable compositions in terms of many ma-

Table 2d. Representative electron microprobe analyses and structural formulae of amphiboles in the Alban Hills ejecta

	P6	P10	P25	P23
SiO_2	36.84	35.87	36.34	34.76
TiO_2	1.16	1.71	1.03	1.55
Al_2O_3	12.87	14.49	13.51	14.01
Cr_2O_3	–	0.03	–	0.02
FeO[a]	24.16	22.66	20.53	26.10
MnO	0.33	0.29	0.84	1.67
MgO	5.99	6.26	7.51	2.70
NiO	–	–	–	0.06
ZnO	–	0.04	–	–
CaO	11.24	11.54	11.54	10.62
SrO	–	–	0.05	0.24
BaO	–	–	0.38	0.13
Na_2O	1.32	1.39	1.54	1.56
K_2O	3.28	2.96	2.66	2.85
Total	97.19	97.24	95.93	96.27
Fe_2O_3[b]	6.11	5.32	6.16	5.36
FeO[b]	18.66	17.87	14.99	21.28
Numbers of ions on the basis of 23 oxygens				
Si	5.831	5.646	5.755	5.675
Al^{IV}	2.169	2.354	2.245	2.325
Al^{VI}	0.232	0.334	0.277	0.371
Ti	0.138	0.202	0.123	0.190
Cr	–	0.004	–	0.003
Fe^{3+}	0.728	0.630	0.734	0.658
Fe^{2+}	2.470	2.353	1.985	2.906
Mn	0.044	0.039	0.113	0.231
Mg	1.413	1.469	1.773	0.657
Ni	–	–	–	0.008
Zn	–	0.005	–	–
Ca	1.906	1.946	1.958	1.858
Sr	–	–	0.005	0.023
Ba	–	–	0.024	–
Na	0.405	0.424	0.473	0.494
K	0.662	0.594	0.537	0.594
mg	0.364	0.384	0.471	0.184
F	0.42	0.34	1.11	0.94
Cl	–	0.02	0.04	0.03

–, Below detection limit
[a] Total Fe as FeO
[b] Calculated according to Droop (1987)

jor components, especially Ca and Na. A high Cl content is observed in P25.

Accessory and secondary phases include apatite, magnetite, pyrrhotite, and fluorite.

Apatite (Table 2g) invariably contains appreciable concentrations of Si, F and SO_3, and can be referred to as F-bearing, silico-sulfate apatite.

Magnetite contains significant amounts of Ti, and, in some cases, Al and Mn. Magnetite from KLT is close to the end-member composition, with a small amount of Cr; however, Cr is very high in magnetites derived from garnet breakdown.

Pyrrhotite is present in samples P10, P6 and P30. In these samples hauyne-nosean and apatite are particularly rich in SO_3. Pyrrhotite occurs as a reaction product of mafic silicate phases. Microprobe analyses of the silicate material in an early stage of transformation gives $SiO_2 \approx 33\%$; $Al_2O_3 \approx 10$; $FeO \approx 25$; $CaO \approx 2$, $Mg \approx O$

Table 2e. Representative electron microprobe analyses and structural formulae of feldspars in the Alban Hills ejecta

	P23	P25	P10	P6
SiO_2	63.49	63.66	63.09	63.48
TiO_2	–	0.17		–
Al_2O_3	19.33	19.13	19.34	19.01
Fe_2O_3[a]	0.26	0.12	–	0.22
MgO	–	–	–	–
CaO	–	–		–
SrO	1.49	1.17	0.95	0.49
BaO	0.22	–	0.53	0.30
Na_2O	2.21	1.64	0.69	0.87
K_2O	12.57	13.90	15.26	15.35
Total	99.57	99.79	99.86	99.72
Numbers of ions on the basis of 32 oxygens				
Si	11.774	11.798	11.770	11.820
Ti	–	0.024	–	–
Al	4.225	4.179	4.252	4.172
Fe^{3+}	0.036	0.017	–	0.031
Mg	–	–	–	–
Ca	–	–	–	
Sr	0.160	0.126	0.103	0.053
Ba	0.016	–	0.039	0.022
Na	0.795	0.589	0.250	0.314
K	2.974	3.286	3.632	3.646

–, Below detection limit
[a] Total Fe as Fe_2O_3

Table 2f. Representative electron microprobe analyses and structural formulae of members of the sodalite group in the Alban Hills ejecta

	P25		P6		P30	
SiO_2	34.03		33.05		31.70	
Al_2O_3	28.92		28.57		27.21	
Fe_2O_3[a]	0.10		0.26		0.38	
MnO	0.17		–		–	
MgO	–		–		0.22	
CaO	4.62		6.39		8.43	
SrO	–		0.27		0.26	
Na_2O	18.97		17.16		13.78	
K_2O	2.91		2.54		5.31	
SO_3	7.70		10.94		12.21	
Cl	2.46		0.80		0.59	
	99.88		99.98		100.09	
$O \equiv Cl$	0.56		0.18		0.13	
Total	99.32		99.80		99.96	
Numbers of ions on the basis of the 21 (0) in the $3Al_2O_3 \cdot 6SiO_2$ framework						
Si	5.996		5.953		5.966	
Al	6.006	12.016	6.064	12.053	6.039	12.059
Fe^{3+}	0.014		0.036		0.054	
Ca	0.872		1.233		1.701	
Sr	–	8.006	0.028	7.836	0.028	8.036
Na	6.480		5.992		5.032	
K	0.654		0.583		1.275	
SO_4	1.019	1.754	1.479	1.724	1.726	1.914
Cl	0.735		0.245		0.188	
	Contains Mn 0.025				Contains Mg 0.062	

–, Below detection limit
[a] Total Fe as Fe_2O_3

Table 2g. Representative electron microprobe analyses and structural formulae of apatites in the Alban Hills ejecta

	KLT		P10		P6		P30	
SiO_2	1.60		1.73		1.83		2.95	
Rare earths	ND		ND		ND		ND	
FeO	0.26		0.02		0.05		0.03	
MnO	–		0.01		0.01		–	
MgO	–		0.01		0.03		0.04	
SrO	2.94		ND		ND		ND	
CaO	52.96		55.33		55.34		55.20	
Na_2O	–		0.07		0.07		0.11	
K_2O	–		0.11		0.04		0.02	
P_2O_5	39.13		38.13		38.37		37.90	
SO_3	0.20		1.76		2.01		1.38	
F	4.42		3.82		2.86		2.91	
Cl	–		0.01		0.03		0.07	
	101.51		101.00		100.64		100.61	
$O \equiv F,Cl$	1.86		1.61		1.21		1.25	
Total	99.65		99.39		99.43		99.36	
Numbers of ions on the basis of 10 (Ca, Mg, etc.)								
Fe	0.037		0.003		0.007		0.004	
Mn	–		0.001		0.001		–	
Mg	–		0.003		0.007		0.010	
Sr	0.291	10.000	–	10.000	–	10.000	–	10.000
Ca	9.672		9.947		9.954		9.947	
Na	–		0.023		0.023		0.035	
K	–		0.023		0.008		0.004	
Si	0.272		0.290		0.308		0.496	
P	5.646	5.944	5.417	5.929	5.454	6.015	5.396	6.066
S	0.026		0.222		0.253		0.174	
F	2.383		2.027		1.518		1.548	
Cl	–		0.003		0.008		0.020	

ND, not determined; –, below detection limit

and K_2O around 1% and $SO_3 = 1.4\%$, which suggests a partial transformation of a mafic silicate mineral by interaction with a S-rich fluid phase.

Geochemistry

Analytical methods

Major element, SO_3, Cl and F data of the studied xenoliths are from Fornaseri (1951), Fornaseri et al. (1963) and Federico (1976), and were determined by classical wet chemical methods. Trace elements Rb, Sr, Zr, Ba, Nb, Y and Ni have been determined by X-ray fluorescence on pure powder rock pellets. Precision (2σ) is better than 5% for Rb, Sr, Zr and Ni and better than 10% for Nb, Y and Ba. The other trace elements have been determined at the Department of Geology, University of Western Ontario, London, Ontario (Canada) by the INAA method described by Gibson and Jagam (1980). Analysis of gamma-ray spectra was done by SAMPO computer program (Routti 1969). Spectral interferences from U fusion products were corrected using factors from Landsberger (1986). In most cases, more than one energy peak of a desired isotope was investigated and a weighted average of concentration is reported. Precision is better than 10% for most elements, except about 15% for Nd and Cs.

The Sr and Nd isotope ratios were determined at the Department of Earth Sciences, University of Rome, on a VG-Micromass 54 E mass spectrometer with on-line computer facilities. Strontium was separated by standard ion exchange techniques and the isotope results are the mean of 350–500 measurements. Average value of NBS 987 standard during the period of study was 0.71024 ± 3 (2σ errors). Neodynium was separated by standard ion exchange techniques, loaded on a triple filament and run as the metal species. The $^{143}Nd/^{144}Nd$ data are normalized to a $^{146}Nd/^{144}Nd$ ratio of 0.7219. Normally, 800 to 1200 ratios per sample were determined. Average values of 0.51183 ± 3 (2σ errors) were obtained on the La Jolla Nd standard.

Results

The obtained geochemical data are reported in Table 3, along with the major, trace element and isotopic compositions of some representative lavas from the Alban Hills and the kamafugitic centres of San Venanzo and Cupaello, NE of the Alban Hills.

The ejecta show very variable major and trace element composition, consistent with the range in modes. The ultramafic samples BD, P34 and P14 have low contents of SiO_2, CaO, alkalies and volatiles (F, Cl, SO_3) and high abundances of MgO and Al_2O_3, reflecting their spinel- and olivine-dominated mineralogy. Samples P6, P10, KLT and P30 have intermediate silica contents and variable compositions in terms of the other major oxides. However, MgO is lower and CaO, K_2O, Na_2O, SO_3 and P_2O_5 higher than in the ultramafic ejecta. Finally, P25 and P23 have high Al_2O_3, Na_2O, K_2O and F and low P_2O_5, CaO, MgO and FeO, in keeping with their feldspar-, nepheline- and leucite-dominated mineralogy,

Table 3. Major (wt%), trace element (ppm) and Sr and Nd isotopic composition of the Alban Hills ejecta, of the Alban Hills lavas Alb10 and Alb13, and of the kamafugitic rocks Ven2 and Cup2A from San Venanzo and Cupaello, Central Italy. Major elements of the ejecta are from Fornasei (1951), Federico (1976). Data on Alban Hills lavas are from Fornaseri et al. (1963) and Peccerillo et al. (1984). Data on kamafugites are from Peccerillo et al. (1988). Isotopic data of samples Alb10, Alb13, Ven2 and Cup2A are from Ferrara et al. (1985) and Holm and Munksgaard (1982) and have been obtained on different samples from the same lava flows

Sample	Alban Hills ejecta						
	BD	P34	P14	P6	KLT	P10	P30
Wt%							
SiO_2	31.10	32.06	34.30	42.49	42.54	44.82	49.17
TiO_2	0.18	0.20	0.50	1.20	0.78	1.00	0.70
Al_2O_3	19.89	16.35	21.29	14.88	12.84	16.68	7.99
Fe_2O_3	2.97	3.21	1.25	6.10	5.15	5.54	1.96
FeO	3.53	4.95	3.35	5.06	2.56	4.35	2.93
MnO	0.18	0.30	0.21	0.18	0.20	0.19	0.16
MgO	40.72	39.54	30.23	4.90	7.73	4.28	11.59
CaO	0.68	3.04	6.14	13.40	16.37	10.82	20.47
Na_2O	0.09	0.49	1.07	1.71	1.13	2.46	0.90
K_2O	0.03	0.22	1.69	7.39	9.13	8.46	3.20
P_2O_5	0.01	0.01	0.02	1.15	0.71	0.79	0.15
LOI	0.10	0.15	0.21	1.50	1.05	1.00	0.70
Total	99.48	100.52	100.26	99.96	100.19	100.39	99.92
SO_3	ND	0.05	0.04	0.73	0.12	0.37	0.50
Cl	ND	0.02	0.01	0.02	0.02	0.14	0.03
F	ND	ND	0.07	0.04	0.09	0.11	0.04
Ppm							
La	18.7	4.7	11.7	60	259	105	58
Ce	34.8	10.5	27.7	142	455	230	124
Nd	12.6	5.9	17.4	75	160	106	62
Sm	1.7	1.5	4.7	18.1	24.1	13.8	13.1
Eu	0.32	0.28	0.98	3.78	4.48	2.91	2.77
Gd	1.47	1.16	3.36	12.24	19.38	9.48	8.87
Tb	0.16	0.17	0.44	1.63	1.79	1.28	1.23
Yb	0.35	0.57	0.92	2.01	1.78	2.23	2.13
Lu	0.05	0.08	0.13	0.28	0.26	0.33	0.28
Y	ND	2	6	29	25	30	30
Cs	0.11	2.82	7.33	103	53	39	11.9
Rb	4	103	170	1059	256	480	110
Ba	108	861	370	350	997	1183	210
Sr	12	177	185	618	1659	2333	1178
Th	23.3	10.9	2.1	21.5	69	51	13.6
U	2.6	0.4	0.5	2.7	13.6	12.0	3.8
Nb	3	7	7	ND	ND	35	ND
Ta	0.38	0.20	0.29	0.40	0.86	1.67	0.40
Zr	53	65	233	349	328	373	247
Hf	1.14	1.16	6.46	14.0	7.33	9.3	8.0
Sb	0.63	0.11	0.11	0.93	1.02	0.65	0.65
Ni	30	27	6	6	90	16	77
Co	13	27	28	41	34	25	29
Cr	1.0	6.6	3.3	1.6	233	8.4	12.4
Sc	3.0	2.7	2.3	8.6	26.8	14.4	69
$^{87}Sr/^{86}Sr$	0.71003±.00003	0.70951±.00003	0.70956±.00002	0.70939±.00003	0.71036±.00003	0.70900±.00005	0.70968±.00002
$^{143}Nd/^{144}Nd$	0.51205±.00002	0.51204±.00002	0.51211±.00002	0.51211±.00002	0.51186±.00002	0.51217±.00002	0.51209±.00002

ND, not detected

the scarcity of apatite and the occurrence of interstitial fluorite.

Ultramafic xenoliths generally have low abundances of rare-earth elements (REE) and many other incompatible trace elements (ITE). However, they also show unusually low concentrations of Cr, Co, Sc and Ni, which sharply contrast with the major element composition and modal mineralogy. The salic samples P25 and P23 have low heavy (H)REE and Hf, but also display extreme enrichment in several other ITE such as Th, light (L)REE, Ta. Again, this latter characteristic is unexpected, given that the modal mineralogy of the rocks

Table 3 (continued)

Sample	P25	P23	Alban Hills lavas		Kamafugites	
			ALB10	ALB13	VEN2	CUP2A
Wt%						
SiO_2	50.54	52.72	46.86	48.18	41.52	43.68
TiO_2	0.13	0.11	1.22	1.09	0.76	1.15
Al_2O_3	23.56	23.77	14.95	14.85	12.08	7.53
Fe_2O_3	1.55	1.35	4.90	2.51	1.68	5.67
FeO	0.98	1.38	3.70	4.79	4.88	2.20
MnO	0.15	0.12	0.31	0.08	0.11	0.12
MgO	0.68	0.54	4.89	7.37	12.76	10.52
CaO	3.64	2.94	10.29	11.81	15.67	14.97
Na_2O	4.17	7.73	1.83	1.20	1.20	0.45
K_2O	13.50	7.90	8.95	6.18	8.36	9.88
P_2O_5	0.02	0.02	0.70	0.48	0.43	1.14
LOI	0.80	1.20	1.80	1.63	0.57	2.90
Total	99.72	99.78	100.40	100.17	100.02	100.21
SO_3	0.27	0.50	–	–	–	–
Cl	0.14	0.06	–	–	–	–
F	0.26	0.47	–	–	–	–
Ppm						
La	147	195	115	97	95	256
Ce	274	303	258	218	191	578
Nd	89	54	–	–	88	232
Sm	5.9	1.5	21	18	20	41
Eu	1.03	0.16	4.0	3.2	3.3	7.6
Gd	2.70	0.95	–	–	–	–
Tb	0.31	0.13	1.90	1.40	1.40	2.90
Yb	0.51	0.14	2.50	2.00	3.10	2.60
Lu	0.08	0.01	0.45	0.45	0.43	0.36
Y	–	–	–	–	41	59
Cs	21.2	1.10	63	44	33	75
Rb	623	87	550	360	462	596
Ba	2023	960	1600	1600	720	4390
Sr	2815	7143	1440	1550	1819	3700
Th	81	84	54	51	38	137
U	15	7.4	–	–	–	–
Nb	20	27	–	–	16	46
Ta	2.07	1.92	0.94	0.84	0.80	3.90
Zr	137	150	–	–	341	825
Hf	3.07	2.15	10.0	8.0	9.2	25
Sb	0.47	1.83	–	–	–	–
Ni	4	ND	46	73	136	80
Co	4.4	1.5	32	33	39	36
Cr	20.5	1.9	16	336	746	50
Sc	0.2	ND	18	33	23	18
$^{87}Sr/^{86}Sr$	0.70943±.00003	0.70966±.00004	0.71037	0.71058	0.71041	0.71128
$^{143}Nd/^{144}Nd$	0.51216±.00002	0.51209±.00002	–	–	–	–

ND, not detected

is dominated by feldspar and foids, which are known to be depleted in Th, Ta, U and LREE (Onuma et al. 1981; Francalanci et al. 1987).

Chondrite-normalized REE patterns are shown in Fig. 3. All the samples have fractionated patterns, sometimes with small negative Eu anomalies, similar to those typically observed in ultrapotassic lavas from the Alban Hills and other Roman volcanoes (e.g., Peccerillo et al. 1984; Conticelli and Peccerillo 1992). Oddly, a negative anomaly is also shown by sample P23 which contains sanidine as the dominant phase and, accordingly, might be expected to show a positive Eu spike. This sample is also noteworthy for its depletion in HREE and for the extreme overall fractionation of REE (La/Yb= 1393).

Figure 4 reports patterns of incompatible elements normalized to the primordial mantle composition of Wood (1979). The ultramafic inclusions have variable fractionation, but all display a negative P and Ti anomaly; sample BD appears to be enriched in Th, U and LREE with respect to other ITE. The intermediate and salic samples have all fractionated patterns with high LILE/HFSE (large-ion-lithophile elements/high-field-strength elements) ratios and negative anomalies of Nb,

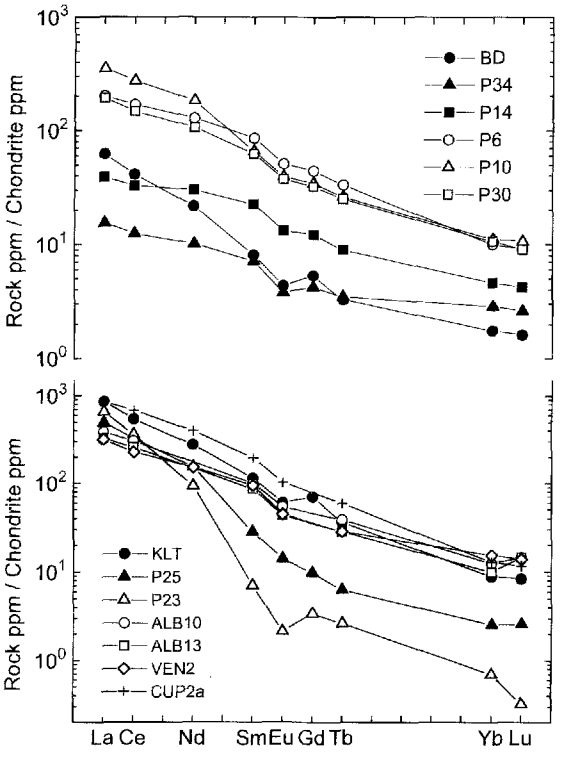

Fig. 3. REE patterns of the Alban Hills ejecta, of some Alban Hills lavas (Alb10, Alb13) and Central Italy kamafugites (Ven2, Cup2a)

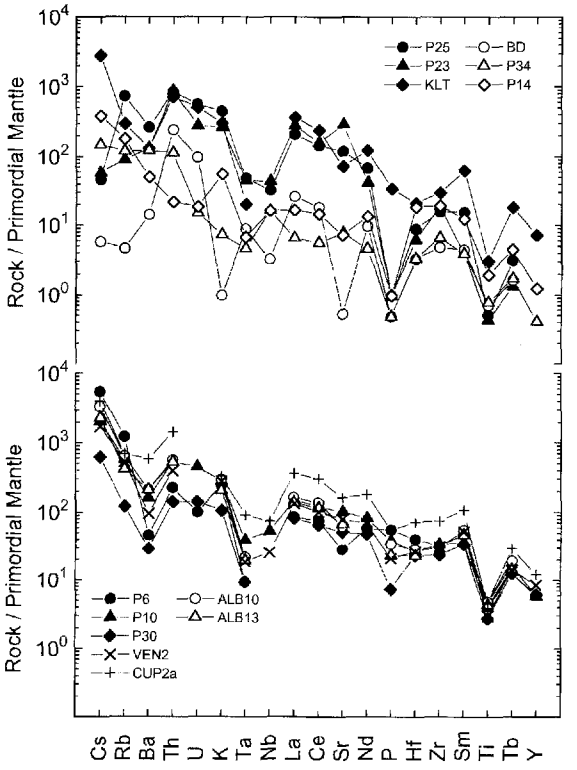

Fig. 4. Incompatible element patterns normalized to a primordial mantle composition of the Alban Hills ejecta and lavas (Alb10, Alb13) and of Central Italy kamafugites (Ven2, Cup2a)

Ta and Ti, which are typical of Roman-type potassic rocks. Negative P spikes are observed in P25, P23 and P30. Note that KLT and P10 have incompatible element patterns which closely match those observed in the Alban Hills lavas and San Venanzo kamafugites (Fig. 4 lower). Also P6 resembles lavas, but has a high concentration of Cs, Rb and K and a slight depletion in Sr.

Strontium isotopic ratios show significant variation (0.70900–0.71036). Except for KLT, all the analyzed ejecta have consistently lower Sr isotopic signatures than the Alban Hills lavas, which range from 0.71024 ± 4 to 0.7109 ± 4 (Ferrara et al. 1985). The Nd isotopic ratios range from 0.51186 to 0.51217. There is a crude negative correlation between Sr and Nd isotopic ratios.

The $\delta^{18}O$ ‰ composition on minerals separated from some of the ejecta studied in this work were determined by Barbieri et al. (1975) and Turi and Taylor (1976). They found that $\delta^{18}O$ ‰ of leucite and clinopyroxene from P30 are +6.7, leucite and clinopyroxene from P6 are +6.7 and +6.9, respectively, and pyroxene and biotite from P14 are +12.6 and +11.5, respectively.

Discussion

Genesis of the Alban Hills ejecta

A number of mechanisms has been invoked to account for the genesis of granular xenoliths occurring in pyroclastic rocks and lavas from the Roman province. Conticelli and Peccerillo (1990) suggested a mantle provenance for spinel-bearing peridotites and dunites in the Torre Alfina lavas, in the northern edge of the Roman province. However, most of the xenoliths so far investigated in the Roman province are thought to have originated within the volcanic system and represent intrusive equivalents of the outcropping lavas, cumulate rocks, thermal metamorphic lithologies and skarns (e.g., Lacroix 1917; Washington 1927; Fornaseri 1951; Hermes and Cornell 1981; Varekamp 1983; Cortini et al. 1985; Turbeville 1992).

Although there is a consensus on the low-pressure origin of the ejecta, considerable debate has been going on regarding the processes that have been responsible for their genesis (e.g., Varekamp 1983; Hermes and Cornell 1983). Accordingly, a preliminary step of the discussion on the studied xenoliths is to place constraints on their genesis, using the mineralogical textural and geochemical evidence previously reported. Successively, the implications of the xenolith study for the understanding of the evolutionary processes within potassic magma chambers will be explored.

Ultramafic ejecta. Textural, and geochemical evidence excludes that any of the analyzed ejecta are of mantle origin. The three ultramafic samples, which are the only candidates to represent mantle lithologies, do not show any of the textural characteristics, such as deformed olivine or granoblastic textures with triple points, which are typically observed in mantle-derived xenoliths (e.g.,

Harte 1977). The very low concentrations of ferromagnasian trace elements such as Cr, Ni and Co also argue against a mantle provenance.

Several lines of evidence also exclude a cumulus origin for the ultramafic xenoliths. These include:
1. The very high MgO contents of olivines (up to Fo_{96}), which rule out a derivation from any magmatic liquid;
2. The low contents of Ni in olivine and, more generally, of all the ferromagnesian trace elements in the whole rocks, which strongly conflicts with the high concentrations of Ni, Cr, Co and Sc found by previous studies in mafic minerals from potassic rocks (Francalanci et al. 1987; Villemant 1988; Francalanci 1989).
3. The lack of compositional zoning in clinopyroxenes, which is one of the most striking characteristics of Roman lavas (e.g., Scott Baldridge et al. 1981; Holm 1982; Aurisicchio et al. 1988), and the high CaO/(FeO + MgO) of these phases, which causes them to fall outside the trend of clinopyroxenes from the Alban Hills lavas on the quadrilateral diagram in Fig. 2.

The most likely possibility is that the ultramafic inclusions derived from interaction between potassic magmas and wall carbonate rocks. Such a hypothesis was suggested by Lacroix (1917) and several other authors (e.g. Barbieri et al. 1975; Varekamp 1983) for ultramafic xenoliths similar to those studied here.

Field and petrological studies on thermally metamorphosed carbonate rocks as well as theoretical investigations of subsolidus equilibria in the $CaO-MgO-SiO_2+CO_2+H_2O$ (CMS) system, representing impure dolomitic limestones, indicate that diopside and forsterite are the end-products of several high-T, low-P metamorphic reactions. The addition of Al_2O_3 to the system (CMAS) may result in the formation of clinochlore and chlorites and, at high temperature, of spinel. Finally, the addition of K_2O (KCMAS) favours crystallization of phlogopite at moderate to high temperatures. Calcite is an almost ubiquitous phase in the metamorphic assemblages at most P–T conditions (Vidale 1969; Myashiro 1973; Winkler 1976; Rice 1977; Alexandrov 1990; Tracy and Frost 1991; Pattison and Tracy 1991).

The range of mineralogical compositions observed in the studied ejecta may be simply explained by a variation in the composition of the protoliths and by a recrystallization at various P–T–X_{CO_2} conditions. The variable physical conditions of the metamorphism can be related to different distance of the rocks from the pluton, even though the absence of calcite requires very low X_{CO_2}, typical of metamorphic rocks crystallized very near to the interface with magmatic bodies (Nicholls 1971; Pattison and Tracy 1991). The compositional variability of the protoliths could be related to initial differences in the sedimentary rocks, but may also derive from infiltration of some components from the magma body, a process recognized around several plutons (e.g., Burnham 1959; Fisher and Wieckman 1991). The relative enrichment in Th, U and LREE of BD (Fig. 4), strongly suggests introduction of chemical components of magmatic origin into the wall rocks. Also Sr isotopic ratios, which are intermediate between values of carbonate rocks (≈ 0.708, Barbieri, unpublished data) and those of the Alban Hills lavas, agree with the hypothesis of an interaction between magma and wall carbonate rocks.

Intermediate and salic ejecta. Intermediate and salic samples have mineral and whole rock composition which indicate that these xenoliths either represent intrusive equivalents of potassic lavas or they result from accumulation of mineral phases at the bottom or on the walls of the magma chamber.

Sample P10 and KLT have major and trace element composition which approaches those of ultrapotassic liquids (Table 2 and Fig. 4). However, while P10 has a composition which closely matches those of leucite tephrites, KLT displays some key major element abundances, such as low Al_2O_3 and Na_2O and very high CaO, which are not found in the Roman-type magmas. These characteristics are typical of ultrapotassic rocks with a kamafugitic affinity, such as those occurring at San Venanzo, NE of Alban Hills (Table 2) (Peccerillo et al. 1988). Note that kalsilite is an important mineral of the San Venanzo kamafugites and is generally absent in typical HKS Roman-type rocks. A genesis at high pressure within the upper mantle (Peccerillo et al. 1988) or, alternatively, a derivation from a Roman-type tephritic magma by moderate amounts of limestone assimilation (Federico 1976) has been invoked in order to explain the extreme undersaturation of these rocks.

Sample P6 has a composition very much like a leucite-tephritic lava, but its high Cs, Rb and K, relative to other LILE, point to a preferential concentration of leucite. High CaO, Sc and Co and SO_3 in sample P30 reflect cumulus clinopyroxene and hauyne-nosean.

Finally, P25 and P23 have high Al_2O_3, K_2O, Na_2O and Sr which reflect concentration of sanidine and nepheline, the dominant phases of these inclusions. However, the extreme concentrations of Th, LREE, and fluorine and the strong REE fractionation in P25 and P23 make the genesis of these ejecta less obvious. A role for cumulus accessory phases is ruled out by petrographic evidence. Moreover, the strong negative spike of P shown by incompatible element patterns (Fig. 4) exclude cumulation of apatite, which is the most common REE-rich accessory phase of Italian potassic rocks.

Detailed microprobe investigations have been carried out in order to identify the phases which contain Th and LREE in P23 and P25. Back-scattered electron images (Fig. 5) revealed the occurrence of very fine grained phases, ten to one hundred microns in size, distributed along the fractures of the main minerals and in the interstices between granules. Semiquantitative EDS analyses (Table 4) indicated that these phases contain variable amounts of P and Si, which vary antipathetically, are rich in Th and LREE, and are likely to be ascribed to britholite, a mineral which is known to form during the pegmatitic stages of magmatic evolution (Haegele and Machatschki 1939). The nature and the interstitial position of this phase clearly reflect a secondary origin, most probably by precipitation from fluids during late- or post-magmatic phases. The occurrence of interstitial fluorite indicates that fluids were rich in fluorine. We suggest that these fluids were able to introduce high

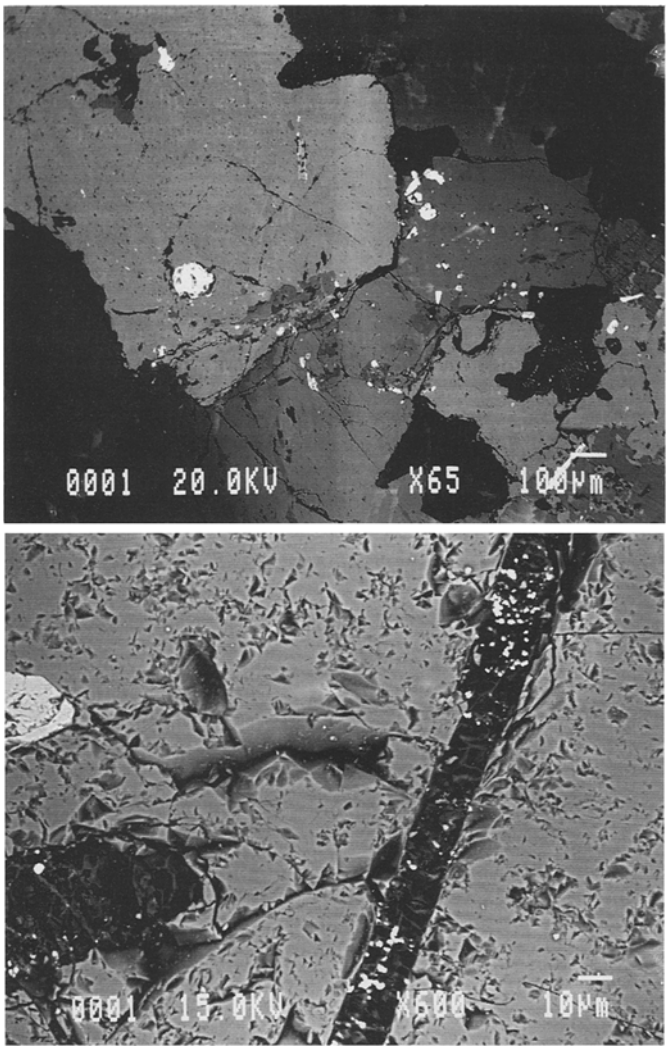

Fig. 5. Back-scattered electron images of P25 (*upper* photograph) and P23 (*lower* photograph) ejecta displaying the Th- and LREE-rich phase, *white spots*, in interstitial position. For semiquantitative analyses of these phases see Table 4. Dark gray minerals are nepheline and sanidine

amounts of Th and LREE in otherwise barren cumulitic rocks.

Contraints on evolutionary processes of ultrapotassic magmas

Geochemical data on the xenoliths from the Alban Hills have shown that interaction between ultrapotassic magma and wall rocks and element mobility by gaseous transfer may have been important processes during the evolution of the Alban Hills magmas. In this section these processes will be further discussed with the aim of providing quantitative constraints on the effects on potassic magmas.

Role of crustal contamination on isotopic heterogeneities. The Alban Hills ejecta have shown lower $^{87}Sr/^{86}Sr$ ratios with respect to the values found by previous studies on

Table 4. Semiquantitative EDS data of Th- and LREE-rich accessory phases of samples P23 and P25

	P23					
P_2O_5	19.2	5.9	34.6	37.0	8.9	17.6
SiO_2	18.1	22.5	7.3	8.8	21.9	13.1
CaO	29.3	19.2	8.7	10.3	18.7	26.0
La_2O_3	11.5	17.2	15.3	16.6	14.0	12.8
Ce_2O_3	19.9	27.3	17.4	20.6	22.3	19.9
Nd_2O_3	1.7	2.2	7.4	3.2	1.8	
ThO_2	–	5.7	9.2	3.5	12.2	10.5

	P25					
P_2O_5	10.1	7.4	13.4	1.6	10.6	24.7
SiO_2	21.8	24.8	16.3	1.8	19.3	14.9
CaO	19.8	20.7	25.9	5.8	23.1	34.5
La_2O_3	13.7	11.8	11.5	40.9	15.2	3.0
Ce_2O_3	21.5	29.2	22.5	6.4	25.5	14.8
Nd_2O_3	1.6	3.6		10.0		
ThO_2	9.6	2.4	10.4		6.3	8.1
Tb_2O_3	1.9	3.4				
V_2O_3				33.4		

lavas (Ferrara et al. 1985). While the $^{87}Sr/^{86}Sr$ ratios of the ultramafic xenoliths are easily justified by envisaging that they reflect isotopic signatures of the basement carbonate rocks, the Sr isotopic composition of the xenoliths of magmatic origin are more difficult to explain and call for additional examination of the genetic hypothesis previously suggested.

In principle, variable Sr and Nd isotope signatures of ejecta and lavas at the Alban Hills may reveal either the occurrence of various batches of magmas generated in a heterogeneous source or a derivation from isotopically homogeneous parental liquids by open-system evolutionary processes. A strong source heterogeneity has been suggested for the Roman province and there is a wide, though not unanimous, consensus that this feature is a result of the introduction into the mantle of variable amounts of upper crustal material by subduction processes (see Conticelli and Peccerillo 1992 and references therein). On the other hand, evidence of interaction between potassic magmas and sedimentary or metamorphic wall rocks has been documented for several potassic volcanoes, including the Alban Hills (e.g., Ferrara et al. 1985; Conticelli and Peccerillo 1990).

Variation of oxygen versus Sr isotopic ratios is an excellent tool to discriminate betweeen source mixing and magma contamination (e.g., Taylor and Sheppard 1986; Ellam and Harmon 1992). Figure 6A reports oxygen versus Sr isotopic relationships for the Alban Hills lavas and xenoliths together with mantle mixing and magma contamination curves. The models clearly indicate that small variations in the amount of upper crustal material added to the mantle generates dramatic modifications of Sr isotopic signatures, whereas $\delta^{18}O$ values are almost unaffected. Accordingly, the most straightforward explanation for the variability of Sr isotopic ratios between Alban Hills lavas and ejecta would be that they

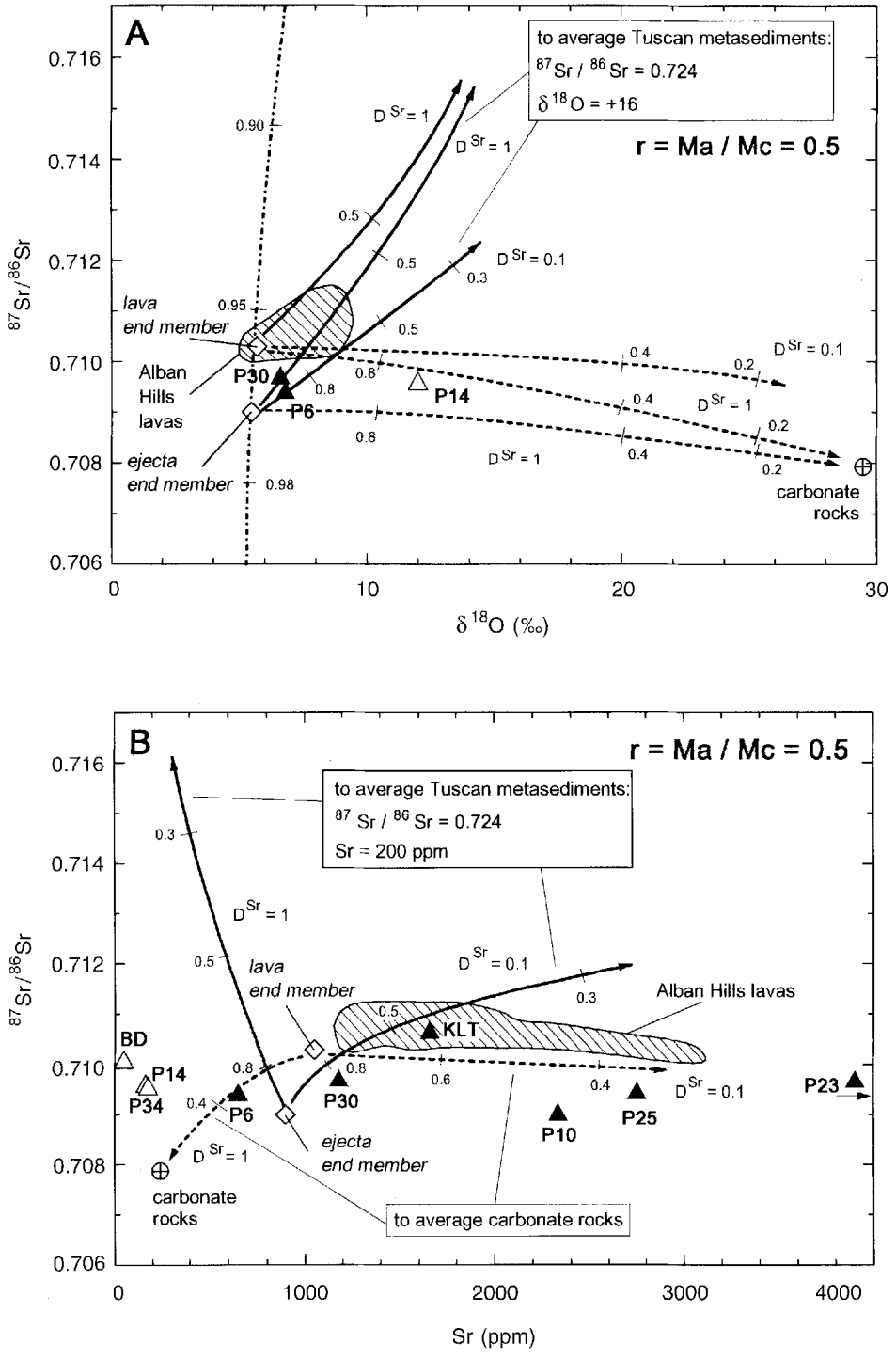

Fig. 6. $^{87}Sr/^{86}Sr$ versus $\delta^{18}O$ ‰ (**A**) and Sr (**B**) relationship for the Alban Hills lavas and ejecta. AFC trends are reported for two hypothetical parental magmas, *diamonds*, with compositions close to that of the isotopically most primitive lavas (*lava end-member*) and ejecta (*ejecta end-member*), which assimilate average metamorphic rocks from Southern Tuscany, Central Italy, *solid lines*, and carbonate rocks, *dashed lines*. Numbers along the AFC lines indicate weight fraction of residual liquid. *Dash-dot* line on $^{87}Sr/^{86}Sr$ versus $\delta^{18}O$ ‰ diagram represents mixing curve of mantle material ($^{87}Sr/^{86}Sr = 0.704$, Sr = 20 ppm; $\delta^{18}O$ ‰ = +6) and Tuscany metamorphic rocks; *numbers* along the trend indicate fraction of mantle material involved in the mixing. $^{87}Sr/^{86}Sr$ and Sr composition of Tuscan metasediments is the mean of the values reported by Pinarelli et al. (1989). Sr abundance of carbonate rocks (Sr = 120 ppm) is the mean of the values reported by Fornaseri and Grandi (1963) on Central Italy carbonate rocks. Sr isotopic ratio of carbonate rocks (0.708) is the mean of unpublished data furnished by Barbieri. Constant oxygen abundances have been assumed in all the models. Data on oxygen isotopic ratios of ejecta, *solid triangles* are from Barbieri et al. (1975) and Turi and Taylor (1976). Oxygen and Sr isotopic data on Alban Hills lavas and on Tuscany rocks are from Ferrara et al. (1985). Oxygen isotope data on carbonate rocks (+30‰) are from Fornaseri and Turi (1969). For further explanation see text

represent independent magma batches generated in a heterogeneous source.

However, a main problem arising from this conclusion is that the analyzed ejecta all come from pyroclastic formations emplaced during the latest stages of the Alban Hills activity. As such, they should represent magmas which were emplaced during previous stages of activity. Instead, lavas have consistently higher Sr isotopic ratios than xenoliths (Ferrara et al. 1985). It could be envisaged that the effusive equivalents of the xenoliths were not sampled and analyzed during previous investigations. However, although this possibility cannot be excluded, it seems unlikely, given the large number of lava samples from different stratigraphic levels which were analyzed by Ferrara et al. (1985).

An alternative hypothesis is that ejecta and lavas represent various stages of evolution of a single type of potassic magma.

Figure 6B shows $^{87}Sr/^{86}Sr$ versus Sr relationships for the studied ejecta and the Alban Hills lavas together with AFC (assimilation-fractional crystallisation) curves for two hypothetical parental magmas. One has a composition close to the least radiogenic lavas (*lava end-member*), the other close to the least radiogenic ejecta (*ejecta end-member*). Average carbonate rocks from Central Italy and average gneisses from Southern Tuscany have been chosen as assimilated material. The ratio r between mass of assimilated and crystallized material has been assumed to be 0.5, since this was found to be a minimum value to have significant $^{87}Sr/^{86}Sr$ variation at low to moderate degrees of evolution.

The models show that if the *lava end-member* is assumed to represent the parental magma, Sr isotopic compositions as those of the ejecta can be obtained by assimilation of carbonate rocks, inasmuch as these have lower Sr isotopic ratios than lavas. However, the lowest Sr isotope values as those of the ejecta are attained only after the liquid has reached about 40% of its initial abundance ($F=0.4$). If the *ejecta end-member* is considered as parental magma, the composition of the most primitive lavas can be modelled by an AFC process that assumes an interaction with Tuscan metamorphic rocks, moderate degrees of evolution ($F=0.7$–0.6), and an incompatible behaviour for Sr ($D_{Sr}=0.1$).

The oxygen isotope data seem to rule out a derivation of ejecta from lavas (Fig. 6A). Interaction between carbonates and the hypothetical *lava end-member* would generate strong variation of oxygen isotope composition which conflicts with the low $\delta^{18}O$ values of the magmatic ejecta. In contrast, the ultramafic sample P14 plots along an AFC curve between the *lava end-member* and carbonate rocks, which substantiates an origin by interaction between magma and carbonates at least for this ultramafic xenolith.

The AFC curves with $D_{Sr}<1$ starting from *ejecta end-member* intersect the field of lavas only at the highest $\delta^{18}O$ values. This leads to rule out a derivation of the lavas from the *ejecta end-member* by AFC process with bulk assimilation of Tuscan rocks. Such a possibility is also excluded by the high ferromagnesian trace element abundances of mafic Alban lavas. In fact, if the realistic assumption is made that the separating mineral assemblage during early stages of evolution is dominated by clinopyroxene and olivine, AFC processes would generate dramatic decrease of ferromagnesian trace elements. For instance, Ni and Cr would drop to a few ppm level, after the liquid has reached 70–60% of its initial mass, if a $D_{s/l}\geq 5$ is assumed for the two elements. This constrasts with the rather high values of Cr and Ni in the most mafic Alban Hills lavas which show abundances of Cr = 100–400 ppm and Ni = 40–100 ppm (Peccerillo et al. 1984).

However, several recent studies have demonstrated that the interaction between magmas and wall rocks may occur via selective assimilation processes (e.g., Dickin 1981; Watson 1982; Grove et al. 1988). Investigations on crustal xenoliths entrained in various types of magmas (e.g., Grove et al. 1988) have shown that biotite is among the first phases to melt when in contact with magmas. Liquids formed by partial melting of granite xenoliths in the Medicine Lake lavas have been found to be low in silica and enriched in MgO, CaO and K and Rb coming from the breakdown of biotite (Grove et al. 1988). It is obvious that the assimilation of these partial melts by mafic magmas may not generate extensive depletion in ferromagnesian elements. Moreover, oxygen isotope compositions of metamorphic biotite (e.g., Garlick and Epstein 1967) resemble closely to those of the Alban Hills magmas. Accordingly, a selective assimilation involving preferential melting of biotite would have little effect on oxygen isotopic composition during AFC.

Role of element transport by fluid phases

The present data provide compelling evidence for high activity of various types of gaseous phases during different stages of magmatic evolution at the Alban Hills. The elevated contents of fluorine in micas, amphiboles and apatites (Table 2) indicate high fluorine contents in the Alban Hills magmas. The high SO_3 in apatites and the abundance of hauyne-nosean in some ejecta testify to high sulfur fugacity during magma crystallization. Moreover, the transformation of silicate phases to pyrrhotite observed in some samples requires the presence of a free, gaseous, S-rich phase which percolated through the walls of the magma chamber generating the metasomatic change of some silicates. Finally, the occurrence of fluorite in some samples represents striking evidence for the presence of circulating fluids during magma evolution.

The association of Th- and LREE-rich, late-magmatic minerals with fluorite in the interstices of P23 and P25, has been interpreted as evidence that the F-rich phase was also responsible for transfer of incompatible elements to the wall rocks. The obtained data can be used to estimate the relative element enrichments during gaseous transfer.

Figure 7 reports ratios of measured versus theoretical abundances for some major and trace elements in samples P23 and P25. Theoretical element abundances of

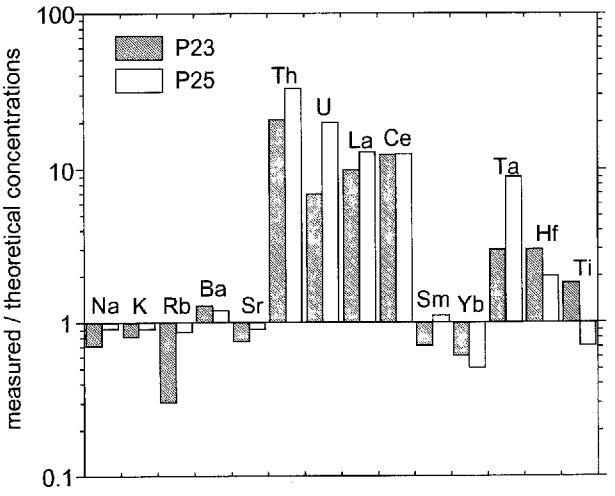

Fig. 7. Ratios of measured versus theoretical abundances of some major and trace elements for salic ejecta P23 and P25. Theoretical compositions have been estimated by mass balance calculations using trace element abundances for the main and accessory phases taken from the literature, major element data from Table 2 and modes from Table 1. Ratios higher than unity indicate selective element enrichment. For further explanation see text

the two samples have been obtained by mass balance calculations using point counted modes of Table 1, major and minor element data on minerals reported in Table 2 and trace element abundances obtained by previous studies on minerals of similar composition from potassic and ultrapotassic rocks (e.g., Onuma et al. 1981; Francalanci et al. 1987; Lemarchand et al. 1987). The plot clearly shows that several elements such as Na, K, Ba, Sr intermediate and heavy REE show minor differences between calculated and measured values for both P23 and P25. This indicates that the abundances of these elements are mainly a function of the mineral phases present in the rock and were not modified by secondary processes. Instead, the measured abundances of Th, U and LREE are higher by an order of magnitude than those expected by mass balance calculations. Tantalum and Hf are also enriched in the rocks, but to a lower degree than Th, U and LREE. Rubidium is close to unity for P25 and lower than unity for P23, which may suggest some loss from the rock.

In conclusion, comparison between calculated and observed element abundances in P25 and P23 indicates that the process of fluid transport was able to determine selective enrichment of Th, U and LREE with respect to other LILE, HREE and HFSE in the wall rocks. Most probably, the fluid was also depleted in Eu, thus balancing or inverting the original positive Eu spike related to the concentration of cumulus sanidine in the rocks.

The most important magmatological implication of this finding is that these fluids also percolated through the liquids residing in the magma chamber, whose composition could have been significantly modified by such a process. The extreme fractionation of REE and the very high enrichments in Th, U and LREE observed in some very evolved phonolitic rocks at the Alban Hills and other Roman volcanoes (e.g., Vico, Barbieri et al. 1988), may derive from fluid transfer phenomena rather than, or in addition to, extreme degrees of fractional crystallization. The high LREE/Ta and Th/Ta values observed in several evolved rocks from the Roman province and the increase of these ratios with increasing differentiation in potassic suites (Barbieri et al. 1988; Villemant 1988) may reflect processes of gaseous transfer. Finally, the LREE- and Th-rich fluorite mineralization common in central Italy (Locardi 1992) are the most impressive effect of the element transfer by F-rich fluids associated with potassic magmas. It is interesting that the bulk REE abundances and fractionation of these mineralizations (Locardi, personal communication) are strikingly similar to those of sample P23.

The origin of F-rich fluid phases is a major problem which, at present, can be only matter for speculation. Villemant (1988) suggested that fluids associated with potassic magmas at the Phlegrean Field derived directly from the upper mantle and interacted with potassic liquids residing in shallow level reservoirs. However, the present study indicates that enrichment in fluorine and ITE only occurs in the most salic ejecta. These rocks essentially consist of sanidine, nepheline and leucite, which are phases that typically crystallize from evolved potassic magmas. It is well known that fluorine has a strong affinity for magmatic liquids and behaves as a highly incompatible element during fractional crystallization (e.g., Bailey and Macdonald 1975; Aoki et al. 1981). Potassic magmas, which contain high concentration of fluorine, may become oversaturated in this element at the most advanced stages of evolution. This leads us to conclude that most probably the F-rich fluid phase derived from the magma chamber by unmixing from potassic liquids during the most advanced stages of evolution.

In summary, the present data provide support to the hypothesis that transfer of incompatible trace elements by gaseous phases may be an important factor during magmatic evolution of alkaline magmas. Bailey and Macdonald (1975, 1987) have suggested that extreme enrichments in ITE in evolved alkaline rocks may be an effect of such a process. The present study strongly supports this hypothesis and also allows the establishment of relative mobility of various ITE. This provides an important tool to constrain element enrichment by gaseous transfer in alkaline magmatic systems.

Conclusions

Mineral chemical, petrological and geochemical data for representative granular ejecta from the Alban Hills pyroclastic deposits provide information on their genesis and on processes occurring within the magma chamber:

1. The ejecta include thermally metamorphosed rocks, intrusive equivalents of the erupted lavas and cumulate rocks. Metamorphic xenoliths are dominated by mafic phases such as olivine, spinel, diopside and phlogopite, which have different compositions to the same phases in the outcropping lavas and in the xenoliths of magmatic origin.

2. Ejecta thought to represent liquid compositions have major and trace element characteristics which reveal the occurrence of ultrapotassic liquids both of Roman and kamafugitic affinity in the Alban Hills. This indicates that kamafugitic (KAM) rocks, previously found only in two localities from Central Italy (San Venanzo and Cupaello), may be more widespread than previously thought and the abundance of KAM rocks may have been underestimated because they are obscured by largely predominant Roman-type potassic and ultrapotassic rocks.
3. Most ejecta have Sr isotopic ratios significantly lower than those of the lavas. This may be interpreted as indicating that ejecta and lavas represent different magma batches. Alternatively, it may be envisaged that ejecta and lavas represent different stages of the evolution of potassic magmas whose isotopic signatures have been modified by interaction with wall rocks within the magma chamber before eruption. This latter hypothesis requires selective assimilation in order to be able to explain fully isotopic and geochemical data.
4. Some xenoliths display evidence of metasomatic modification of silicate phases to pyrrothite. Others have exceedingly high abundances of incompatible elements such as Th, U, LREE and extreme REE fractionation which are not justified by their mineralogical composition (dominant sanidine and foids with minor garnet and amphiboles). These latter ejecta also contain fluorite and secondary minerals rich in Th and LREE which occur interstitially between mineral grains or along the fractures of the main minerals. Overall, these data highlight the role of element transport by the fluid phase within potassic magma chambers. They also allow the establishment of relative mobilities of various ITE in alkaline potassic systems.

Acknowledgements. The authors express their appreciation to R. Macdonald, University of Lancaster, for the critical reading of an early draft of the manuscript and to two anonymous referees for constructive reviews. The assistance of Francesca Castorina, Enrico di Biaso and M. Serracino during isotopic and microprobe analyses of F-bearing phases is gratefully acknowledged. G. Crisci, University of Calabria, and L. Parrini, University of Florence, kindly provided some X-ray fluorescence data. P. Mandò and Alba Santo, University of Florence, kindly carried out PIXE measurements on olivines. Financial support is from MURST (40%) and CNR, "CS Geologia del quaternario ed evoluzione ambientale", Rome, and project on "Petrology, geochemistry and mineralogy of magmatic rocks from orogenic environments", Messina.

References

Alexandrov SM (1990) Geochemistry of skarn and ore formation in dolomites (in Russian). Nauka, Moskow

Aoki K, Ishicawa K, Kanisawa S (1981) Fluorine geochemistry of basaltic rocks from continental and oceanic regions and petrogenetic implications. Contrib Mineral Petrol 76:53–59

Aurisicchio C, Federico M (1985) Nepheline-kalsilite microperthites in ejecta from the Alban Hills (Italy). Bull Geol Soc Finl 57:5–12

Aurisicchio C, Federico M, Gianfagna A (1988) Clinopyroxene chemistry of the high-potassium suite from the Alban Hills, Italy. Mineral and Petrol 39:1–19

Bailey SW (1984) Classification and structures of the micas. In: Bailey SW (ed) Reviews in mineralogy 13. Mineral Soc Am, Washington DC, pp 1–12

Bailey DK, MacDonald R (1975) Fluorine and chlorine in peralkaline liquids and the need for magma generation in an open system. Mineral Mag 40:405–414

Bailey DK, MacDonald R (1987) Dry peralkaline felsic liquids and carbon dioxide flux through the Kenya rift zone. In: Mysen BO (ed) Magmatic processes: physicochemical principles. Geochem Soc Spec Publ 1, pp 91–105

Barbieri M, Penta A, Turi B (1975) Oxygen and strontium isotope ratios in some ejecta from the Alban Hills volcanic area, Roman Comagmatic Region. Contrib Mineral Petrol 51:127–133

Barbieri M, Peccerillo A, Poli G, Tolomeo L (1988) Major, trace element and Sr isotopic composition of lavas from Vico volcano (Central Italy) and their evolution in an open system. Contrib Mineral Petrol 99:485–497

Bernardi A, De Rita D, Funiciello R, Innocenti F, Villa IM (1982) Chronology and structural evolution of Alban Hills volcanic complex, Latium, Italy (abstract). 5th Int Conf Geochronol, Cosmochronol Isotope Geol, Nikko, Japan, 23–24 July 1982

Burnham CW (1959) Contact metamorphism of magnesian limestones at Crestmore, California. Geol Soc Am Bull 70:879–920

Conticelli S, Peccerillo A (1990) Petrological significance of high-pressure ultramafic xenoliths from ultrapotassic rocks of Central Italy. Lithos 24:305–322

Conticelli S, Peccerillo A (1992) Petrology and geochemistry of potassic and ultrapotassic volcanism from Central Italy: inferences on its genesis and on the mantle source evolution. Lithos 28:221–240

Cortini M, Lima A, De Vivo B (1985) Trapping temperatures of melt inclusions from ejected vesuvian mafic xenoliths. J Volcanol Geothermal Res 26:167–172

Cundari A (1982) Petrology of clinopyroxenite ejecta from Somma-Vesuvius and ther genetic implications. Tschermaks Mineral Petrogr Mitt 30:17–35

De Rita D, Funiciello R, Parotto M (1988) Geological map of the Colli Albani volcanic complex. Scale 1:50,000. CNR, Gruppo Naz Vulcanol, Roma

Dickin AP (1981) Isotope geochemistry of Tertiary igneous rocks from the Isle of Skye, NW Scotland. J Petrol 22:155–189

Droop GTR (1987) A general equation for estimating Fe^{3+} concentrations in ferromagnasian silicates and oxides from microprobe analyses using stoichiometric criteria. Mineral Mag 51:431–435

Ellam RM, Cox KG (1991) An interpretation of Karoo picrite basalt in terms of interaction between asthenospheric magmas and the mantle lithosphere. Earth Planet Sci Lett 105:330–342

Ellam RM, Harmon RS (1990) Oxygen isotope constraints on the crustal contributions to the subduction-related magmatism of the Aeolian islands, southern Italy. J Volcanol Geothermal Res 44:105–122

Federico M (1976) On a kalsilitolite from the Alban Hills, Italy. Period Mineral 45:5–12

Federico M, Gianfagna A, Zanazzi PF (1988) A zirconium-bearing fassaite from the Alban Hills, Italy. Neues Jahrb Mineral Monatsh 1988:495–502

Ferguson AK (1978) Ca-enrichment in olivine from volcanic rocks. Lithos 11:189–194

Ferrara G, Laurenzi MA, Taylor HP, Tonarini S, Turi B (1985) Oxygen and strontium isotope studies of K-rich volcanic rocks from the Alban Hills, Italy. Earth Planet Sci Lett 75:13–28

Fisher GW, Wieckmann MJ (1991) Computer simulation of mineral zonation in infiltration skarn, Crestmore, California (abstract). Geol Soc Am Program Abstr 23:112

Foley SF (1992) Vein-plus-wall-rock melting mechanisms in the lithosphere and the origin of potassic alkaline magmas. Lithos 28:435–453

Fornaseri M (1951) Ricerche petrografiche sul Vulcano Laziale. I. Proietti inclusi nei tufi. Period Mineral 20:211–235

Fornaseri M, Grandi L (1963) Contenuto in stronzio di serie calcaree italiane. G Geol 31:171–198

Fornaseri M, Turi B (1969) Carbon and oxygen isotopic composition of carbonates in lavas and ejectites from the Alban Hills, Italy. Contrib Mineral Petrol 23:244–256
Fornaseri M, Scherillo A, Ventriglia U (1963) La regione vulcanica dei Colli Albani. CNR, Roma
Francalanci L (1989) Trace element partition coefficients for minerals in shoshonitic and calcalkaline rocks from Stromboli Island (Aeolian Arc). Neues Jahrb Mineral Abh 160:229–247
Francalanci L, Peccerillo A, Poli G (1987) Partition coefficients for minerals in potassium-alkaline rocks: data from Roman province (Central Italy). Geochem J 21:1–10
Funiciello R, Parotto M (1978) Il substrato sedimentario nell'area dei Colli Albani: considerazioni geodinamiche e paleogeografiche sul margine Tirrenico dell'Appennino Centrale. Geol Romana 17:233–248
Garlick GD, Epstein S (1967) Oxygen isotope ratios in coexisting minerals of regionally metamorphosed rocks. Geochim Cosmochim Acta 31:181–214
Gianfagna A (1985) Occurrence of baddeleyte – ZrO_2 – in an ejected block from Colle Cimino, Marino (Alban Hills, Italy). Period Mineral 54:129–133
Gibson IL, Jagam P (1980) Instrumental neutron activation analysis of rocks and minerals. In: Muecke GK (ed) Neutron activation analysis in the geosciences, short course. Mineral Assoc Can, pp 109–131
Grove TL, Kinzler RJ, Baker MB, Donnelly-Nolan JM, Lesher CE (1988) Assimilation of granite by basaltic magma at Burnt lava flow, Medicine Lake volcano, northern California: decoupling of heat and mass transfer. Contrib Mineral Petrol 99:320–343
Haegele G, Machatschki F (1939) Der Britholith ist ein cererden silikatapatil. Zentralbl Mineral 1939:165–167
Harte B (1977) Rock nomenclature with particular relation to deformation and recrystallization textures in olivine-bearing xenoliths. J Geol 85:279–288
Hermes OD, Cornell WC (1981) Quenched crystal mush and associated magma compositions as indicated by intercumulus glasses. J Volcanol Geothermal Res 9:133–149
Hermes OD, Cornell WC (1983) The significance of mafic nodules in the ultra-potassic rocks from central Italy – reply. J Volcanol Geothermal Res 16:166–172
Holm PM (1982) Mineral chemistry of perpotassic lavas of the Vulsinian district, the Roman Province, Italy. Mineral Mag 46:379–386
Holm PM, Munksgaard NC (1982) Evidence for mantle metasomatism: an oxygen and strontium isotope study of the Vulsinian district, central Italy. Earth Planet Sci Lett 60:376–388
Lacroix A (1917) Les formed grenues du magma leucitique du Volcan Laziale. C R Accad Sci Paris 165:1029–1034
Landsberger S (1986) Spectral interferences from uranium fission in neutron activation analysis. Chem Geol 57:415–421
Leake BE (1978) Nomenclature of amphiboles. Can Mineral 16:501–520
Lemarchand F, Villemant B, Calas G (1987) Trace element distribution coefficients in alkaline series. Geochim Cosmochim Acta 51:1071–1081
Lloyd FE, Bailey DK (1975) Light element metasomatism of the continental mantle: the evidence and the consequences. Phys Chem Earth 9:389–416
Locardi E (1992) Minerogenesi di origine mantellica nell'Appennino. Rend Fis Accad Lincei, Rome 2:239–251
Miyashiro A (1973) Metamorphism and metamorphic belts. Allen and Unwin, London
Nelson DR (1992) Isotopic characteristics of potassic rocks: evidence for the involvement of subducted sediments in magma genesis. Lithos 28:403–420
Nicholls IA (1971) Calcareous inclusions in lavas and agglomerates of Santorini volcano. Contrib Mineral Petrol 30:261–276
Onuma N, Ninomiya S, Nagasawa H (1981) Mineral/groundmass partition coefficients for nepheline, melilite, clinopyroxene and perovskite in melilite-nepheline basalts, Nyiragongo, Zaire. Geochem J 15:221–228
Papike JJ, Cameron KL, Baldwin K (1974) Amphiboles and pyroxenes: characterization of other than quadrilateral components and estimates of ferric iron from microprobe data (abstract). Geol Soc Am Program Abstr 6:1053–1054
Pattison DMR, Tracy RJ (1991) Phase equilibria and thermobarometry of metapelites. In: Kerrick DM (ed) Reviews in mineralogy 26. Mineral Soc Am, Washington DC, pp 105–206
Peccerillo A (1990) On the origin of the Italian potassic magmas – Comments. Chem Geol 85:183–196
Peccerillo A, Poli G, Tolomeo L (1984) Genesis, evolution and tectonic significance of K-rich volcanics from the Alban Hills (Roman Comagmatic Region) as inferred from trace element geochemistry. Contrib Mineral Petrol 86:230–240
Peccerillo A, Poli G, Serri G (1988) Petrogenesis of orenditic and kamafugitic rocks from Central Italy. Can Mineral 26:45–65
Pinarelli L, Poli G, Santo AP (1989) Geochemical characterization of Recent volcanism from the Tuscan magmatic province (Central Italy): the Roccastrada and San Vincenzo centers. Period Mineral 59:67–96
Rice JM (1977) Progressive metamorphism of impure dolomitic limestones in the Marysville aureole, Montana. Am J Sci 277:1–24
Rittmann A (1933) Die geologische bedingte Evolution und Differentiation des Somma-Vesuvmagmas. Z Vulkanol 15:8–94
Routti JT (1969) SAMPO, a FORTRAN program for computer analysis of gamma spectra from Ge(Li) detectors and for the other spectra with peaks. Lawrence Radiat Lab Rep UCRL-19542, Univ California, Berkeley
Santo AP, Peccerillo A, Del Carmine P, Lucarelli F, MacArthur JD, Mandò PA (1992) External PIXE and micro-PIXE measurements of elemental concentrations in volcanic rocks. Nucl Instrum Methods Phys Res B64:517–522
Scott Baldridge W, Carmichael ISE, Albee AL (1981) Crystallization path of leucite-bearing lavas: examples from Italy. Contrib Mineral Petrol 76:321–335
Taylor HP, Sheppard SMF (1986) Igneous rocks: processes of isotopic fractionation and isotope systematics. In: Valley JW, Taylor HP, O'Neil JR (eds) Reviews in mineralogy 16. Mineral Soc Am, Washington DC, pp 227–318
Tracy RJ, Frost BR (1991) Phase equilibria and thermobarometry of calcareous, ultramafic and mafic rocks, and iron formations. In: Kerrick DM (ed) Reviews in mineralogy 26. Mineral Soc Am, Washington DC, pp 207–289
Turbeville BN (1992) Relationship between chamber margin accumulates and pore liquids: evidence from arrested in situ processes in ejecta, Latera caldera, Italy. Contrib Mineral Petrol 110:429–441
Turi B, Taylor HP (1976) Oxygen isotope studies of potassic volcanic rocks of the Roman province, central Italy. Contrib Mineral Petrol 55:1–31
Varekamp JC (1983) The significance of mafic nodules in the ultra-potassic rocks from central Italy – Discussion. J Volcanol Geothermal Res 16:161–165
Vidale R (1969) Metasomatism in a chemical gradient and the formation of calc-silicate bands. Am J Sci 267:857–874
Villemant B (1988) Trace element evolution in the Phlegrean Fields (central Italy): fractional crystallization and selective enrichment. Contrib Mineral Petrol 98:169–183
Vollmer R (1989) On the origin of the Italian potassic magmas. 1. A discussion contribution. Chem Geol 74:229–239
Washington HS (1927) The italite locality of Villa Senni. Am J Sci 14:173–198
Watson BE (1982) Basalt contamination by continental crust: some experiments and models. Contrib Mineral Petrol 80:73–87
Winkler HGF (1976) Petrogenesis of metamorphic rocks. Springer Verlag, Berlin Heidelberg New York
Wood DA (1979) A variably veined suboceanic upper mantle. Genetic significance for mid-ocean ridge basalts from geochemical evidence. Geology 7:499–503

Editorial responsibility: J. Hoefs